

LETTER TO THE EDITOR

Stellar mass estimates in early-type galaxies from lensing+dynamical and photometric measurements

C. Grillo^{1,2}, R. Gobat¹, P. Rosati¹, and M. Lombardi^{1,2}

¹ European Southern Observatory, Karl-Schwarzschild-Str. 2, D-85748, Garching bei München, Germany
e-mail: cgrillo@eso.org

² Università degli Studi di Milano, Department of Physics, via Celoria 16, I-20133 Milan, Italy

Received X X, X; accepted Y Y, Y

ABSTRACT

Aims. To compare two different diagnostics for estimating stellar masses in early-type galaxies and to establish their level of reliability. In particular, we consider the well-studied sample of 15 field elliptical galaxies selected from the Sloan Lens ACS (SLACS) Survey ($z = 0.06 - 0.33$). We examine here the correlation between the stellar mass values, enclosed inside the Einstein radius (R_{Ein}) of each lens, based on analyses of lensing and stellar dynamics combined and based on multiwavelength photometry spectral template fitting.

Methods. The lensing+dynamics stellar mass $M_{\text{len+dyn}}^* (\leq R_{\text{Ein}})$ is obtained from the published SLACS Survey results, assuming a two-component density distribution model and a prior from the fundamental plane on the mass-to-light ratio for the lens galaxies. The photometric stellar mass $M_{\text{phot}}^* (\leq R_{\text{Ein}})$ is measured by fitting the observed spectral energy distribution of the galaxies (from the SDSS multi-band photometry over 354 – 913 nm) with composite stellar population templates, under the assumption that light traces stellar mass.

Results. The two methods are completely independent. They rely on several different assumptions, and so, in principle, both can have significant biases. Based on our sample of massive galaxies ($\log M_{\text{phot}}^* (\leq R_{\text{Ein}}) \approx [10.3, 11.5]$), we find consistency between the values of $M_{\text{len+dyn}}^* (\leq R_{\text{Ein}})$ and $M_{\text{phot}}^* (\leq R_{\text{Ein}})$. We obtain a Pearson linear correlation coefficient of 0.94 and a median value of the ratio between the former and the latter mass measurements of 1.1 ± 0.1 . This suggests that both methods can separately yield reliable stellar masses of early-type galaxies, and confirms that photometric mass estimates are accurate, as long as optical/near-IR rest frame photometry is available.

Key words. galaxies: elliptical and lenticular, cD – galaxy: formation – galaxy: evolution – gravitational lensing – galaxies: kinematics and dynamics – cosmology: observations

1. Introduction

An estimate of the stellar mass component in galaxies is interesting for several different reasons. In detail, by combining or comparing photometric stellar mass estimates, obtained by spectral energy distribution (SED) fitting methods, with dynamical or lensing measurements, it is possible to study the radial distribution of dark matter (e.g., Ferreras et al. 2005; Napolitano et al. 2005), to investigate the relationship between stellar and total mass (e.g., Lintott et al. 2006; Rettura et al. 2006), and to test hierarchical structure formation models (e.g., Nagamine et al. 2004; De Lucia et al. 2006). Interestingly, Treu & Koopmans (2004) have proved that the stellar mass fraction in elliptical lens galaxies can also be estimated with a joint lensing and dynamical analysis.

Although it is common to measure stellar masses through these techniques, only a few studies have been performed to check the reliability of each method (e.g., Drory et al. 2004). Further investigations are therefore important to probe the consistency of the different techniques.

Throughout this work we assume $H_0 = 70 \text{ km s}^{-1} \text{ Mpc}^{-1}$, $\Omega_m = 0.3$, and $\Omega_\Lambda = 0.7$.

2. The SLACS sample

In this Letter, we focus on a uniformly selected sample of 15 massive field early-type galaxies taken from the SLACS Survey (for more details on the selection procedure, see Bolton et al. 2006). Table 1 summarizes the relevant photometric and spectroscopic properties of the galaxy sample. The lens galaxies have a redshift between 0.06 and 0.33, *HST* F435W and F814W images, *ugriz* magnitudes and stellar velocity dispersions from the SDSS¹. They are luminous red galaxies (LRG; Eisenstein et al. 2001) with properties similar to those of non-lensing early-type galaxies: redshifts, stellar velocity dispersions, stellar populations, and mass density profiles (see Treu et al. 2006; Koopmans et al. 2006).

3. Measuring stellar masses

Here, we describe how the stellar mass of the galaxies of our sample is measured using two independent diagnostics.

3.1. Lensing+dynamical estimates

Strong gravitational lensing provides the most accurate estimate of the total (stellar+dark) projected mass of a lens galaxy inside the Einstein radius. It has been shown by Treu & Koopmans (2004) that by combining lensing measurements with spatially resolved kinematic profiles in elliptical galaxies, the stellar and dark components can be separated precisely. If the velocity dispersion of stars is known only from a single (fiber) aperture, some information on the stellar mass fraction (f_*) inside R_{Ein} can still be obtained. This particular analysis has been performed on the SLACS sample by Koopmans et al. (2006). The results are shown in Table 2. We summarize here the main steps and assumptions:

- The mass distribution of each lens galaxy is described in terms of a two-component spherical and isotropic model. It consists of a Hernquist density profile, scaled by a stellar mass-to-light ratio M_*/L , for the stellar component, and a power-law density profile, for the dark matter component ($\rho_d = \rho_{d,0} r^{-\gamma}$).
- The lensing measurement of the total projected mass enclosed inside the Einstein circle, $M_{\text{len+dyn}}^{\text{tot}} (\leq R_{\text{Ein}})$, is used to eliminate $\rho_{d,0}$. Thus, for any given set $\{M_*/L, \gamma\}$, the spherical Jeans equation can be solved to determine the line-of-sight stellar velocity dispersion as a function of radius.
- A likelihood function is defined by comparing the model predicted with the observed aperture stellar velocity dispersion. A prior on the stellar mass-to-light ratio, based on the fundamental plane (in the B band) and corrected for passive evolution, is considered before marginalizing on the two free parameters of the model (M_*/L and γ).
- The stellar mass fraction is calculated as the ratio between the maximum likelihood and the maximum allowed values of M_*/L . This latter quantity is obtained under the assumption that $M_{\text{len+dyn}}^* (\leq R_{\text{Ein}}) = M_{\text{len+dyn}}^{\text{tot}} (\leq R_{\text{Ein}})$.

In principle, this method can give values of f_* bigger than 1, as can be seen in a few cases in Table 2. Nevertheless, these values are consistent with 1, so that the previous assumptions are not in doubt. Finally, Koopmans et al. (2006) point out that more realistic values of M_*/L should take into account the dependence on the mass of the galaxy.

The stellar mass obtained from the combination of gravitational lensing and stellar dynamics measurements inside the Einstein radius, $M_{\text{len+dyn}}^* (\leq R_{\text{Ein}})$, is then estimated by multiplying the total mass by the stellar mass fraction. This is shown in the following equation

$$M_{\text{len+dyn}}^* (\leq R_{\text{Ein}}) = f_* \times M_{\text{len+dyn}}^{\text{tot}} (\leq R_{\text{Ein}}), \quad (1)$$

and the results for the SLACS sample (Koopmans et al. 2006) are reported in Table 2.

3.2. Photometric estimates

The flux of our galaxies has been measured in five different bands (see Table 1), from 354 to 913 nm ($ugriz$ filters of the SDSS). In order to obtain unbiased galaxy colors, in the absence of color gradients, a de Vaucouleurs profile,

$$I(R) = I_0 \exp\left[-7.67 \left(\frac{R}{R_e}\right)^{1/4}\right] \quad (2)$$

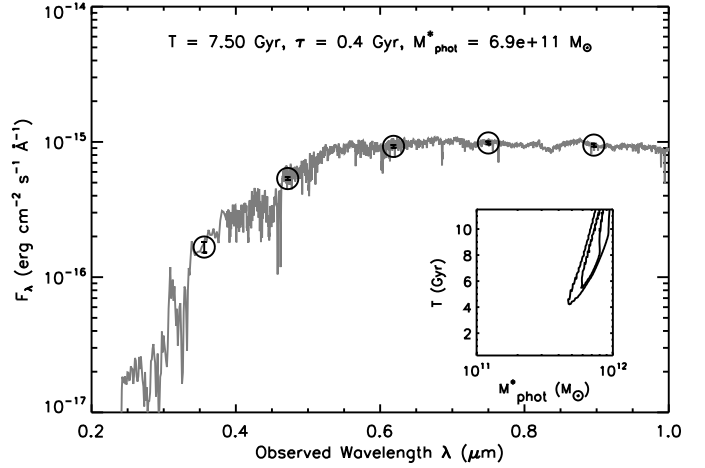


Fig. 1. SED and best-fit model of the lens galaxy SDSS J0912+0029 at $z = 0.1642$. The circles with the error bars represent, from left to right, the observed total flux densities measured in the u , g , r , i , and z SDSS passbands. On the top, the best-fit values of the age (T), the characteristic time of the SFH (τ), and the mass (M_{phot}^*) of the galaxy are given. On the bottom right, the inset shows the 68% and 99% confidence regions for T and M_{phot}^* .

(R_e being the standard optical effective radius), is fitted in the r band of each object and this model is then varied, only in amplitude, for the other bands (after convolution with the corresponding point spread function). The resulting magnitudes are called modelMag in the publicly available SDSS catalog and correspond to magnitudes measured through equivalent apertures in all bands.

We derive the total photometric stellar mass (M_{phot}^*) by fitting the observed SED with a three-parameter grid of composite stellar population (CSP) models. We use Bruzual & Charlot’s (2003) templates at solar metallicity, assuming a Salpeter (1955) time-independent initial mass function (IMF) and a delayed exponential star formation history (SFH) parametrized by a characteristic timescale (τ). The other two free parameters are the age of the model (T), which is constrained by the age of the Universe at the galaxy redshift, and the stellar mass. The uncertainties on the best-fit parameters are estimated by projecting the joint probability density distribution onto the corresponding axes. As an example, Fig. 1 shows the SED of a galaxy in our sample and the best-fit model. The estimated stellar mass values are given in Table 2. We emphasize that the accuracy and homogeneity of the SDSS photometry, particularly the lack of significant systematics due to calibration or aperture corrections, ensure accurate photometric mass estimates.

The photometric stellar mass inside the Einstein radius, $M_{\text{phot}}^* (\leq R_{\text{Ein}})$, of Table 2 is inferred by multiplying the total mass by an aperture factor (f_{ap}):

$$M_{\text{phot}}^* (\leq R_{\text{Ein}}) = f_{\text{ap}} \times M_{\text{phot}}^* \quad (3)$$

This last factor represents the fraction of light enclosed inside the Einstein radius, with respect to the total light of the galaxy parametrized by the de Vaucouleurs profile, and is explicitly given by the following expression:

$$f_{\text{ap}} = \frac{\int_0^{R_{\text{Ein}}} I(R) R dR}{\int_0^\infty I(R) R dR} \quad (4)$$

The assumption implicit in using Eq. (3) is that the stellar mass is traced by the light distribution.

Finally, we note that stellar mass estimates depend on the adopted IMF and SFH, but not on the different stellar population models (e.g. Bruzual & Charlot 2003 vs. Maraston 2005). We will come back to these points in the next section.

4. Comments and conclusions

In Fig. 2, we compare our photometric stellar mass estimates with the lensing+dynamics ones of Koopmans et al. (2006). This plot shows that the two different mass measurements are statistically correlated and consistent within the error bars. In particular, the value of the Pearson linear correlation coefficient is $\rho = 0.94$, and the best-fit correlation line yields:

$$M_{\text{lens+dyn}}^*(\leq R_{\text{Ein}}) = 10^{2.30 \pm 1.68} \times M_{\text{phot}}^*(\leq R_{\text{Ein}})^{0.80 \pm 0.15}. \quad (5)$$

The median value of the ratio (q) between the lensing+dynamical and photometric stellar mass estimates is consistent with unity (1.1 ± 0.1). The ratio q does not show any correlation with galaxy colors, hence excluding a possible source of systematic errors in the photometric mass estimates.

No significant difference in the relation between $M_{\text{lens+dyn}}^*(\leq R_{\text{Ein}})$ and $M_{\text{phot}}^*(\leq R_{\text{Ein}})$ is observed deriving photometric stellar masses with Maraston's (2005) CSP models, as the two stellar population models differ remarkably in a near-IR regime at wavelengths longer than the ones probed by the SDSS filters. This result is in agreement with that reported by Rettura et al. (2006). By choosing Kroupa (2001) or Chabrier's (2003) IMFs, the photometric mass measurements are lowered in such a way that the slope of the best fit is consistent with that of Fig. 2, but the average ratio between the two mass estimates is considerably smaller than one. Moreover, we note that the effect of contamination caused by the lensed objects in the measurements of the fluxes of a lens galaxy is small. This is usually more relevant in the bluer filters, which are known to be less sensitive to photometric mass estimates, and the measurements of total magnitudes through de Vaucouleurs profile fitting should further reduce this source of uncertainty.

Values of q slightly larger than one, like those observed and shown in the inset of Fig. 2, may be explained by possible underestimates of $M_{\text{phot}}^*(\leq R_{\text{Ein}})$, which can be ascribed to two different phenomena occurring in the galaxies: dust extinction and metallicity values lower than the solar one. In detail, both effects tend to give lower IR fluxes, which then result in lower mass estimates. Nevertheless, several tests have supported the validity of the dust-free and solar metallicity model assumptions (e.g., see Rettura et al. 2006).

Finally, despite a number of assumptions, we conclude that the good agreement between the two mass estimators, within their respective uncertainties, is a very reassuring result. This makes the presence of strong biases in one of the two methods very unlikely, and allows us to use either of them independently to measure reliably stellar masses. Although this study is based on a low redshift sample, we expect photometric mass estimates to be also accurate to high redshift, as long as the same optical/near-IR rest frame bands are covered.

Acknowledgements.

We thank G. Bertin for useful comments on this manuscript. We acknowledge the use of data from the accurate SDSS database. The SDSS Web Site is <http://www.sdss.org/>.

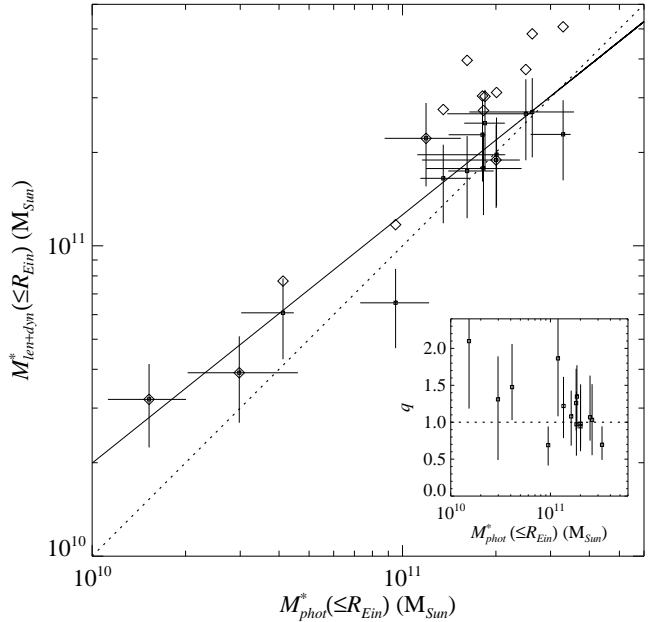


Fig. 2. Comparison of the lensing+dynamical and photometric stellar masses (measured inside the Einstein radii) for the SLACS sample of gravitational lens early-type galaxies. The plot shows $M_{\text{lens+dyn}}^*(\leq R_{\text{Ein}})$ vs. $M_{\text{phot}}^*(\leq R_{\text{Ein}})$, with the best fit correlation (solid) and the $M_{\text{lens+dyn}}^*(\leq R_{\text{Ein}}) = M_{\text{phot}}^*(\leq R_{\text{Ein}})$ (dotted) lines. The diamonds indicate upper limits for the lensing+dynamical stellar masses obtained by assuming that the measured masses enclosed inside the Einstein circles are only stellar. In the inset, we plot the ratio (q) between the lensing+dynamical and photometric stellar mass estimates as a function of $M_{\text{phot}}^*(\leq R_{\text{Ein}})$.

References

- Bolton A. S., Burles S., Koopmans L. V. E., Treu T., and Moustakas L. A. 2006, *ApJ*, 638, 703
- Bruzual G. & Charlot S. 2003, *MNRAS*, 344, 1000
- Chabrier G. 2003, *PASP*, 115, 763
- De Lucia G., Springel V., White S. D. M., Croton D., and Kauffmann G. 2006, *MNRAS*, 366, 499
- Drory N., Bender R., and Hopp U. 2004, *ApJ*, 616, 103
- Eisenstein D. J., Annis J., Gunn J., et al. 2001, *AJ*, 122, 2267
- Ferreras I., Saha P., and Williams L. L. R. 2005, *ApJ*, 623, 5
- Koopmans L. V. E., Treu T., Bolton A. S., Burles S., and Moustakas L. A. 2006, *ApJ*, 649, 599
- Kroupa P. 2001, *MNRAS*, 322, 231
- Lintott C. J., Ferreras I., and Lahav O. 2006, *ApJ*, 648, 826
- Maraston C. 2005, *MNRAS*, 362, 799
- Nagamine K., Cen R., Hernquist L., et al. 2004, *ApJ*, 610, 45
- Napolitano N. R., Capaccioli M., Romanowsky A. J., et al. 2005, *MNRAS*, 357, 691
- Rettura A., Rosati P., Strazzullo V., et al. 2006, *A&A*, 458, 717
- Salpeter E. E. 1955, *ApJ*, 121, 161
- Treu T. & Koopmans L. V. E. 2004, *ApJ*, 611, 739
- Treu T., Koopmans L. V. E., Bolton A. S., Burles S., and Moustakas L. A. 2006, *ApJ*, 640, 662

Table 1. The relevant spectroscopic and photometric measurements of the SLACS sample.

SDSS Name	z	R_e ($''$)	R_{Ein} ($''$)	u (mag)	g (mag)	r (mag)	i (mag)	z (mag)
J0037-0942	0.1955	2.38 ± 0.02	1.47	19.740 ± 0.127	18.038 ± 0.010	16.807 ± 0.006	16.339 ± 0.006	16.013 ± 0.016
J0216-0813	0.3317	3.37 ± 0.22	1.15	21.034 ± 0.335	19.124 ± 0.024	17.455 ± 0.009	16.860 ± 0.009	16.593 ± 0.021
J0737+3216	0.3223	3.26 ± 0.13	1.03	21.200 ± 0.266	19.400 ± 0.025	17.834 ± 0.010	17.214 ± 0.008	16.892 ± 0.020
J0912+0029	0.1642	4.81 ± 0.02	1.61	19.287 ± 0.063	17.410 ± 0.007	16.228 ± 0.004	15.746 ± 0.004	15.399 ± 0.008
J0956+5100	0.2405	2.60 ± 0.03	1.32	20.134 ± 0.136	18.475 ± 0.012	17.129 ± 0.007	16.632 ± 0.006	16.267 ± 0.013
J0959+0410	0.1260	1.82 ± 0.05	1.00	20.363 ± 0.088	18.697 ± 0.012	17.639 ± 0.007	17.169 ± 0.006	16.783 ± 0.016
J1250+0523	0.2318	1.77 ± 0.01	1.15	19.943 ± 0.084	18.500 ± 0.012	17.256 ± 0.007	16.732 ± 0.006	16.484 ± 0.014
J1330-0148	0.0808	1.23 ± 0.01	0.85	20.060 ± 0.081	18.371 ± 0.009	17.442 ± 0.006	17.063 ± 0.007	16.742 ± 0.015
J1402+6321	0.2046	3.14 ± 0.02	1.39	20.353 ± 0.142	18.294 ± 0.011	16.952 ± 0.006	16.444 ± 0.005	16.097 ± 0.011
J1420+6019	0.0629	2.60 ± 0.10	1.04	18.156 ± 0.025	16.386 ± 0.004	15.541 ± 0.003	15.153 ± 0.003	14.889 ± 0.016
J1627-0053	0.2076	2.14 ± 0.02	1.21	20.583 ± 0.190	18.588 ± 0.017	17.286 ± 0.008	16.805 ± 0.008	16.510 ± 0.017
J1630+4520	0.2479	2.02 ± 0.02	1.81	20.554 ± 0.138	18.876 ± 0.015	17.396 ± 0.007	16.861 ± 0.007	16.561 ± 0.014
J2300+0022	0.2285	1.80 ± 0.01	1.25	20.476 ± 0.190	19.007 ± 0.017	17.647 ± 0.009	17.126 ± 0.008	16.803 ± 0.022
J2303+1422	0.1553	4.20 ± 0.04	1.64	19.427 ± 0.194	17.562 ± 0.012	16.385 ± 0.006	15.907 ± 0.006	15.605 ± 0.014
J2321-0939	0.0819	4.47 ± 0.01	1.57	18.045 ± 0.037	16.145 ± 0.004	15.200 ± 0.003	14.772 ± 0.003	14.478 ± 0.006

Notes – Magnitudes are extinction-corrected modelMag (AB) from the SDSS.

References – Treu et al. (2006); Koopmans et al. (2006).

Table 2. The lensing+dynamical and photometric mass measurements of the SLACS sample.

SDSS Name	$M_{\text{len+dyn}}^{\text{tot}}(\leq R_{\text{Ein}})$ ($10^{10} M_{\odot}$)	f_*	M_{phot}^* ($10^{10} M_{\odot}$)	f_{ap}	$M_{\text{len+dyn}}^*(\leq R_{\text{Ein}})$ ($10^{10} M_{\odot}$)	$M_{\text{phot}}^*(\leq R_{\text{Ein}})$ ($10^{10} M_{\odot}$)
J0037-0942	27.3	0.65 ± 0.19	49^{+16}_{-17}	0.37	18 ± 5	18^{+6}_{-6}
J0216-0813	48.2	0.56 ± 0.16	110^{+40}_{-41}	0.24	27 ± 8	26^{+10}_{-10}
J0737+3216	31.2	0.63 ± 0.20	90^{+6}_{-40}	0.22	20 ± 6	20^{+1}_{-9}
J0912+0029	39.6	0.44 ± 0.13	69^{+15}_{-9}	0.23	17 ± 5	16^{+4}_{-2}
J0956+5100	37.0	0.72 ± 0.21	77^{+4}_{-34}	0.32	27 ± 8	25^{+1}_{-11}
J0959+0410	7.7	0.79 ± 0.23	12^{+1}_{-3}	0.34	6 ± 2	4^{+1}_{-1}
J1250+0523	18.9	1.04 ± 0.30	52^{+10}_{-22}	0.39	19 ± 6	20^{+4}_{-8}
J1330-0148	3.2	1.05 ± 0.30	4^{+1}_{-1}	0.40	3 ± 1	2^{+1}_{-1}
J1402+6321	30.3	0.82 ± 0.23	63^{+10}_{-9}	0.29	25 ± 7	18^{+3}_{-3}
J1420+6019	3.9	1.08 ± 0.31	11^{+6}_{-9}	0.27	4 ± 1	3^{+2}_{-1}
J1627-0053	22.2	1.04 ± 0.30	34^{+10}_{-9}	0.35	22 ± 7	12^{+4}_{-3}
J1630+4520	50.8	0.45 ± 0.13	70^{+4}_{-15}	0.47	23 ± 7	33^{+2}_{-7}
J2300+0022	30.4	0.75 ± 0.22	45^{+1}_{-10}	0.40	23 ± 7	18^{+1}_{-4}
J2303+1422	27.5	0.60 ± 0.17	51^{+10}_{-8}	0.27	17 ± 5	14^{+4}_{-2}
J2321-0939	11.7	0.56 ± 0.16	39^{+11}_{-9}	0.24	7 ± 2	9^{+3}_{-2}

References – Koopmans et al. (2006).